Slow relaxation dynamics in binary glasses during stress-controlled, tension-compression cyclic loading

Nikolai V. Priezjev*

Department of Mechanical and Materials Engineering, Wright State University, Dayton, OH 45435, United States
National Research University Higher School of Economics, Moscow 101000, Russia

ARTICLE INFO

ABSTRACT

The effect of cyclic loading on relaxation dynamics and mechanical properties of metallic glasses is studied using molecular dynamics simulations. We consider the Kob-Andersen three-dimensional binary mixture rapidly cooled across the glass transition and subjected to thousands of tension-compression cycles in the elastic range. It was found that during cyclic loading at constant pressure, the system is relocated to progressively lower levels of the potential energy, thus promoting greater densification and higher strength. Furthermore, with increasing stress amplitude, the average glass density increases and the minimum of the potential energy becomes deeper, while the elastic modulus is reduced. The typical size of clusters of atoms with large nonaffine displacements becomes smaller over consecutive cycles, which correlates with the gradual decrease in the potential energy. These results are important for thermomechanical processing of metallic glasses with improved mechanical properties.

1. Introduction

Understanding the quantitative correlation between atomic structure and mechanical and physical properties of amorphous materials such as metallic glasses is important for various structural and biomedical applications [1]. It is commonly accepted that deformation of amorphous materials occurs via a series of sudden rearrangements of small groups of particles often called shear transformation zones [2–4]. Interestingly, it was recently demonstrated that the shear modulus as well as local shear transformations can be accurately predicted using the 'flexibility volume', a parameter that combines the information of both static atomic volume and thermal vibrations [5]. The results of atomistic simulations of cyclic nanoindentation of metallic glasses have revealed hardening effects that arise due to local stiffening and densification of the region containing the original yielding path [6–9]. It was also shown that upon cyclic compression, an amorphous frictional granular matter approaches an asymptotic configuration with maximal volume fraction, and the universal reduction in dissipation is determined by frictional losses and changes in the neighbor list [10,11]. However, the influence of complex deformation protocol and sample preparation history on fatigue lifetime, structural changes, and yielding requires further investigation.

Recent molecular dynamics simulation studies of the fatigue mechanism in metallic glasses under tension-compression, strain-controlled cyclic loading revealed that a shear band is initiated at the sample surface due to a slow accumulation of shear transformation zones, followed by a relatively quick propagation of a shear band across the sample [12,13]. In contrast, the results of atomistic simulations of metallic glasses under the uniaxial stress-control mode have shown that the plastic deformation in small-size samples proceeds via network-like shear-transition zones [14]. Furthermore, it was demonstrated that low-cycle fatigue tests on metallic glass nanowires result in work hardening or softening, depending on the applied load, and, after strain-dependent microscopic damage accumulation, a shear band forms rapidly [15,16]. More recently, it was also found that well-annealed metallic glasses, subjected to periodic compressive stress below yield, exhibit softening with either decreasing cycling frequency or increasing stress amplitude [17]. Despite extensive efforts, however, how exactly the yielding transition and shear band formation depend on the cyclic loading conditions (stress versus strain controlled), frequency, and system size remains not fully understood.

In recent years, the mechanical response of amorphous materials subjected to periodic shear was extensively studied using either athermal, quasistatic [18–24] or finite temperature [25–33] molecular dynamics simulations. Under cyclic loading, athermal systems were shown to settle into the so-called limit cycles, where all particles return to their positions after one or several shear cycles [19,20]. Moreover, the number of shear cycles required to reach a steady state increases upon approaching the yield strain from below [18–20]. Above the yield point, periodic deformation of well-annealed glasses results in sudden

---

formation of a system-spanning shear band after a number of transient cycles and in an increase of the potential energy [12,22,29]. Remarkably, it was recently demonstrated that in contrast to dense amorphous systems, where the yielding transition is associated with a drop of the elastic modulus and enhanced particle diffusion, weakly jammed solids exhibit two-step yielding process; namely, softening at intermediate strain amplitudes and the onset of diffusion at distinctly larger yield strain [30].

In this paper, we investigate mechanical properties and structural relaxation dynamics of poorly annealed binary glasses under periodic tension-compression, stress-controlled loading using molecular dynamics simulations. It will be shown that during several thousand cycles in the elastic range, the amorphous systems continue to explore progressively lower potential energy states and become more dense. The slow relaxation process is associated with small-scale irreversible particle rearrangements that are facilitated by the applied loading. As the stress amplitude increases, the average glass density becomes larger and both the potential energy and elastic modulus are reduced.

The rest of the paper is structured as follows. The details of the molecular dynamics simulation model and the stress-controlled cyclic loading protocol are described in the next section. The numerical results for the time dependence of the potential energy, glass density, and elastic modulus as well as the analysis of nonaffine displacements are presented in Section 3. The main results are briefly summarized in the last section.

2. Details of MD simulations

Molecular dynamics simulations are carried out on a glass former that consists of the non-additive binary mixture (80:20) first introduced by Kob and Andersen (KA) [34] to study properties of the amorphous metal alloy $Ni_{80}P_{20}$ [35]. In this model, the interaction between atoms of types $\alpha, \beta = A, B$ is given by the pairwise Lennard-Jones (LJ) potential:

$$V_{\alpha\beta}(r) = 4\varepsilon_{\alpha\beta}\left[\left(\frac{\sigma_{\alpha\beta}}{r}\right)^{12} - \left(\frac{\sigma_{\alpha\beta}}{r}\right)^{6}\right], \tag{1}$$

where $\varepsilon_{\alpha\beta}$ and $\sigma_{\alpha\beta}$ are the energy and length scales of the LJ potential [36]. The interaction parameters for both types of atoms are chosen as follows: $\varepsilon_{AA} = 1.0$, $\varepsilon_{AB} = 1.5$, $\varepsilon_{BB} = 0.5$, $\sigma_{AB} = 0.8$, $\sigma_{BB} = 0.88$, and $m_A = m_B$ [34]. In addition, the cutoff radius is set to $r_{c,\alpha\beta} = 2.5\sigma_{\alpha\beta}$ to improve computational efficiency. All physical quantities are expressed in the reduced LJ units of length, mass, energy, and time, which are defined as $\sigma = \sigma_{AA}$, $m = m_A$, $\varepsilon = \varepsilon_{AA}$, and $\tau = \sigma\sqrt{m/\varepsilon}$, respectively. The total number of atoms throughout the study is $N_{tot} = 40,000$. The equations of motion were integrated using the velocity Verlet algorithm [36] with the time step $\Delta t_{MD} = 0.005\tau$ using the LAMMPS numerical code [37].

We next describe the preparation procedure and the stress-controlled deformation protocol at constant pressure. The system was initially equilibrated at the temperature $1.1\varepsilon/k_B$ and constant volume, which corresponds to the atomic density $\rho = \rho_A + \rho_B = 1.2\sigma^{-3}$. Here, k_B denotes the Boltzmann constant. This temperature is well above the glass transition temperature of the KA model at the density $\rho = 1.2\sigma^{-3}$ [34]. In the next step, the temperature was instantaneously reduced to $T_{LJ} = 0.1\varepsilon/k_B$ below the glass transition, and the pressure along the $\hat{x}$ and $\hat{y}$ directions was set to zero. In contrast, the normal stress along the $\hat{z}$ direction was varied periodically with the period of oscillations $T = 500\tau$. More specifically, the normal stress σ_{zz} was changed piecewise linearly as follows: from 0 to σ_{zz}^{max} during $T/4$, from σ_{zz}^{max} to $-\sigma_{zz}^{max}$ during $T/2$, and from $-\sigma_{zz}^{max}$ back to 0 during $T/4$. Thus, the average of σ_{zz} over the oscillation period is zero, and the system was subjected to 5000 stress-controlled, tension-compression cycles. In all simulations, periodic boundary conditions were applied along the $\hat{x}$, $\hat{y}$, and $\hat{z}$ directions. The data for the potential energy, stresses, system dimensions,
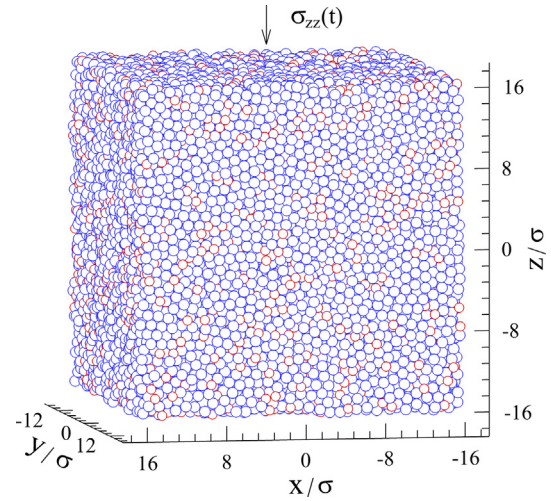

Fig. 1. A snapshot of the Lennard-Jones binary glass ($N_{tot} = 40,000$) after the quench to the temperature $T_{LJ} = 0.1\varepsilon/k_B$. The time-dependent stress $\sigma_{zz}(t)$ is applied along the $\hat{z}$ direction, while the normal stresses along the $\hat{x}$ and $\hat{y}$ directions are kept constant (see text for details). Note that atoms of types A and B (indicated by blue and red circles) are now shown to scale. (For interpretation of the references to color in this figure legend, the reader is referred to the web version of this article.)

and atomic configurations were collected in one sample for the post-processing analysis (see Fig. 1).

3. Results

As described in the previous section, the normal stress in the $\hat{z}$ direction was applied piecewise linearly in time with the oscillation period $T = 500\tau$. As an example, the actual stress σ_{zz} measured in MD simulations during the first 5 cycles after the thermal quench to the temperature $T_{LJ} = 0.1\varepsilon/k_B$ is presented in Fig. 2 for two values of the stress amplitude. As expected, it can be seen that the stress variation is linear with superimposed fluctuations during the consecutive time intervals. Note also that in the case $\sigma_{zz}^{max} = 0.8\varepsilon\sigma^{-3}$, the stress becomes slightly smaller than the value $-0.8\varepsilon\sigma^{-3}$, when the sample is at maximum tension. It should be emphasized that due to periodic boundary conditions in the transverse directions, it is expected that a shear band
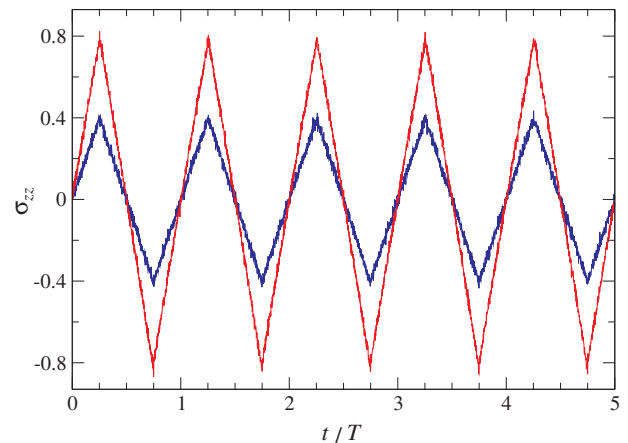

Fig. 2. The time series of the normal stress σ_{zz} (in units of $\varepsilon\sigma^{-3}$) during the first 5 periods after the thermal quench to the temperature $T_{LJ} = 0.1\varepsilon/k_B$. The stress amplitude is $\sigma_{zz}^{max} = 0.4\varepsilon\sigma^{-3}$ (blue lines) and $\sigma_{zz}^{max} = 0.8\varepsilon\sigma^{-3}$ (red lines). The oscillation period is $T = 500\tau$. (For interpretation of the references to color in this figure legend, the reader is referred to the web version of this article.)
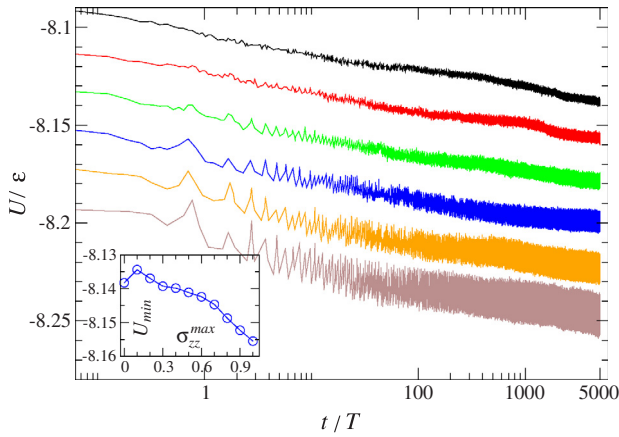
Fig. 3. The potential energy per atom U/ε during 5000 tension-compression cycles after the thermal quench for different stress amplitudes. The data are displaced by -0.02ε for $\sigma_{zz}^{max} = 0.2\varepsilon\sigma^{-3}$ (red), by -0.04ε for $\sigma_{zz}^{max} = 0.4\varepsilon\sigma^{-3}$ (green), by -0.06ε for $\sigma_{zz}^{max} = 0.6\varepsilon\sigma^{-3}$ (blue), by -0.08ε for $\sigma_{zz}^{max} = 0.8\varepsilon\sigma^{-3}$ (orange), and by -0.10ε for $\sigma_{zz}^{max} = 1.0\varepsilon\sigma^{-3}$ (brown). The data for $\sigma_{zz}^{max} = 0$ are indicated by the black curve. The inset shows the average U_{min}, computed after 5000 cycles, as a function of the stress amplitude σ_{zz}^{max}. The period of oscillations is $T = 500\tau$ and the temperature is $T_{LJ} = 0.1\varepsilon/k_B$. (For interpretation of the references to color in this figure legend, the reader is referred to the web version of this article.)

will be formed in a plane perpendicular to the loading direction at sufficiently large strain amplitudes (not considered in the present study). In order to observe the formation of shear bands at about 45° with respect to the loading direction, the simulation cell must have non-periodic boundary conditions in at least one of the transverse directions [12].

The variation of the potential energy as a function of time is shown in Fig. 3 for the stress amplitudes $\sigma_{zz}^{max}\sigma^3/\varepsilon = 0$, 0.2, 0.4, 0.6, 0.8, and 1.0. It becomes apparent, when plotted on the log scale, that in all cases the potential energy decreases monotonically during the whole time interval of 5000 cycles, thus slowly approaching the level of energy minimum. Note that similar results for the potential energy series were reported for periodically sheared glasses at constant volume and sufficiently high temperatures $T_{LJ} \geqslant 0.01\varepsilon/k_B$ in the elastic range [32,33], while at lower temperatures and in athermal systems, the potential energy levels off after about 100 shear cycles near the critical strain amplitude [18,19,32]. Typically, the number of cycles required to reach a steady state decreases when the strain amplitude is reduced away from the critical value [18,19,22,32].

The upper black curve in Fig. 3 denotes the data for $\sigma_{zz}^{max} = 0$, *i.e.*, it represents a physical aging process at constant pressure applied in all three dimensions, which leads to progressively lower energy states and higher glass density (discussed below). It was demonstrated previously that, when the temperature of the KA mixture is reduced below the glass transition and the system is allowed to evolve at constant volume, the potential energy decreases as a power-law function of time and the two-times correlation functions exhibit strong time and waiting time dependence [38,39]. Furthermore, as shown in Fig. 3, with increasing stress amplitude, the minimum of the potential energy becomes deeper and the amplitude of the energy oscillations increases. Note that in order to avoid overlap between different curves, the data are displaced vertically in Fig. 3. The average value of the potential energy after 5000 cycles was estimated as follows. After the last cycle, the pressure was set to zero in all three dimensions (*i.e.*, $\sigma_{zz}^{max} = 0$) and the system was allowed to relax during $10^4\tau$. Thus, the average value of the potential energy during the time interval $10^4\tau$ is reported in the inset to Fig. 3. It can be seen that periodic loading with larger stress amplitudes results in lower values of the potential energy.

Next, the time evolution of the average glass density is plotted in Fig. 4 for the indicated stress amplitudes. It is evident that both quiescent glass at constant pressure and periodically stressed glasses
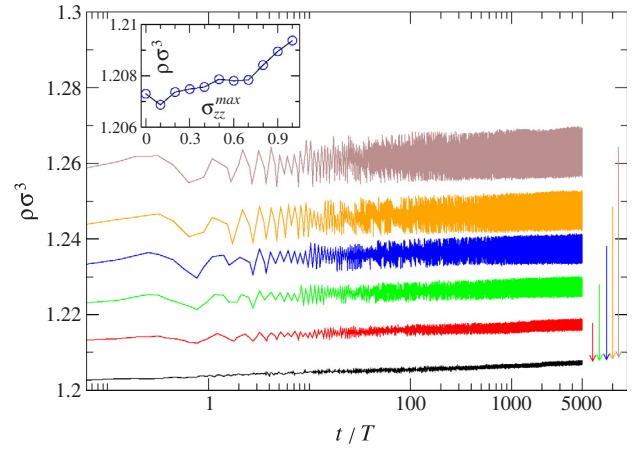

Fig. 4. The time dependence of the glass density, $\rho\sigma^3$, during 5000 cycles for the stress amplitudes $\sigma_{zz}^{max}\sigma^3/\varepsilon = 0.0$, 0.2, 0.4, 0.6, 0.8, and 1.0 (from bottom to top). For clarity, the data are displaced vertically by $+0.01\sigma^3$ for $\sigma_{zz}^{max} = 0.2\varepsilon\sigma^{-3}$ (red), by $+0.02\sigma^3$ for $\sigma_{zz}^{max} = 0.4\varepsilon\sigma^{-3}$ (green), by $+0.03\sigma^3$ for $\sigma_{zz}^{max} = 0.6\varepsilon\sigma^{-3}$ (blue), by $+0.04\sigma^3$ for $\sigma_{zz}^{max} = 0.8\varepsilon\sigma^{-3}$ (orange), and by $+0.055\sigma^3$ for $\sigma_{zz}^{max} = 1.0\varepsilon\sigma^{-3}$ (brown). The vertical displacements of the data are marked by the arrows. The inset shows the average glass density after 5000 cycles as a function of the stress amplitude (see text for details). (For interpretation of the references to color in this figure legend, the reader is referred to the web version of this article.)

become more dense over time. Similar to the potential energy, the average glass density was extracted from the data during the additional time interval of $10^4\tau$ at constant (zero) pressure after 5000 cycles. The results are summarized in the inset in Fig. 4. It can be observed that the long-time average density becomes larger with increasing strain amplitude. Over many cycles, the more efficient packing at higher strain amplitudes is achieved because groups of atoms can rearrange more easily when a system is under tension, thus leading to lower energy states at higher densities. Note, however, that the glass density at zero pressure in the quiescent sample is slightly lower than at the strain amplitude $\sigma_{zz}^{max}\sigma^3/\varepsilon = 0.01$, as shown in the inset to Fig. 4. Most probably this behavior can be ascribed to a particular realization of disorder.

The time dependence of the elastic modulus, E, is reported in Fig. 5 for the selected strain amplitudes. In our study, the modulus was computed simply as a ratio of the stress amplitude and the strain amplitude for every cycle. As can be seen, E increases on average as a function of time for each stress amplitude. Note that the data are more noisy at smaller stress amplitudes. Furthermore, the inset in Fig. 5 shows E, averaged over the last 100 cycles, versus the stress amplitude σ_{zz}^{max}. Although the data are somewhat scattered, the trend is evident; namely, the elastic modulus decreases at larger stress amplitudes. These results are consistent with conclusions from the previous MD study on periodically sheared binary glasses at constant volume, where it was found that, with increasing strain amplitude up to a critical value, the potential energy slightly decreases but at the same time the storage modulus is also reduced [33]. This trend can be rationalized by realizing that, when the strain amplitude increases, nonaffine displacements of atoms become increasingly broadly distributed in strained samples, leading to a local stress relaxation and a decrease in the elastic modulus [28].

We next analyze the spatial distribution of atoms with large nonaffine displacements after a full cycle. To remind, the nonaffine measure is computed numerically using the transformation matrix $\mathbf{J}_i$, which linearly transforms the positions of neighboring atoms during the time interval Δt and minimizes the quantity $D^2(t, \Delta t)$ in the following expression [4]:

$$D^2(t, \Delta t) = \frac{1}{N_i}\sum_{j=1}^{N_i}\{\mathbf{r}_j(t+\Delta t) - \mathbf{r}_i(t+\Delta t) - \mathbf{J}_i[\mathbf{r}_j(t) - \mathbf{r}_i(t)]\}^2,$$
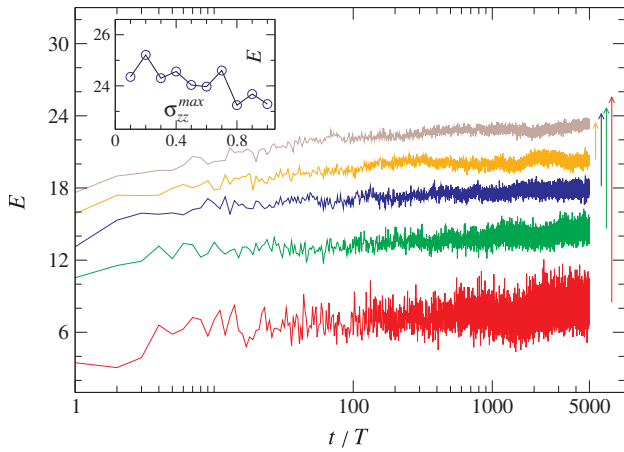
$$(2)$$

Fig. 5. The variation of the elastic modulus, E (in units of $\varepsilon\sigma^{-3}$), during 5000 cycles for the stress amplitudes $\sigma_{zz}^{max}\sigma^3/\varepsilon = 0.2,\ 0.4,\ 0.6,\ 0.8,$ and 1.0 (from bottom to top). The data are shifted by $-17.0\varepsilon\sigma^{-3}$ for $\sigma_{zz}^{max}\sigma^3/\varepsilon = 0.2$ (red), by $-10.0\varepsilon\sigma^{-3}$ for $\sigma_{zz}^{max}\sigma^3/\varepsilon = 0.4$ (green), by $-6.0\varepsilon\sigma^{-3}$ for $\sigma_{zz}^{max}\sigma^3/\varepsilon = 0.6$ (blue), and by $-3.0\varepsilon\sigma^{-3}$ for $\sigma_{zz}^{max}\sigma^3/\varepsilon = 0.8$ (orange). The offsets are indicated by the vertical arrows. The brown curve indicates the original data for $\sigma_{zz}^{max}\sigma^3/\varepsilon = 1.0$. The inset shows E after 5000 cycles versus σ_{zz}^{max}. (For interpretation of the references to color in this figure legend, the reader is referred to the web version of this article.)

where the sum is taken over nearest neighbors within the cutoff distance of 1.5σ from the position of the i-th atom $\mathbf{r}_i(t)$. Based on the previous analysis, it is expected that at sufficiently low temperatures, the system starts to deform reversibly after a number of transient cycles, and the nonaffine displacements of atoms after a full cycle will be

smaller than the cage size [32]. In contrast, above the critical strain amplitude, it was found that in steady state of deformation at finite temperature, a significant fraction of atoms undergo large nonaffine displacements after a full cycle and form a system-spanning shear band in both well [29] and poorly [33] annealed glasses.

The consecutive snapshots of atomic positions with large nonaffine displacements are displayed in Fig. 6 for the stress amplitude $\sigma_{zz}^{max} = 0.2\varepsilon\sigma^{-3}$ and in Fig. 7 for $\sigma_{zz}^{max} = 1.0\varepsilon\sigma^{-3}$. In each case, the nonaffine measure, Eq. (2), was computed for atomic configurations at the beginning and at the end of a cycle when the applied stress is zero, *i.e.*, $\Delta t = T$. It can be seen from Figs. 6(a) and 7(a) that after the first ten oscillation periods following the thermal quench, the atoms with relatively large nonaffine displacements, $D^2(9T, T) > 0.04\sigma^2$, form a number of compact clusters. After hundreds of cycles, the irreversible rearrangements become rare and they mostly consist of isolated smaller (type B) atoms that are more mobile. We note that the presence of a finite number of atoms with large nonaffine displacements after 5000 cycles [see Figs. 6(d) and 7(d)] is consistent with the continuing decay of the potential energy and glass densification shown in Figs. 3 and 4, respectively. In other words, as the number of cycles increases up to 5000, the system continues to explore states with lower potential energy via occasional irreversible rearrangements of small groups of atoms. Finally, the absence of a shear band that consists of atoms with large nonaffine displacements during the time interval $5000\,T$ confirms that the system deforms elastically even at the largest stress amplitude considered in the present study.

4. Conclusions

In summary, the influence of the stress-controlled, tension-compression cyclic loading on mechanical properties of binary glasses was examined using molecular dynamics simulations. The model glass was
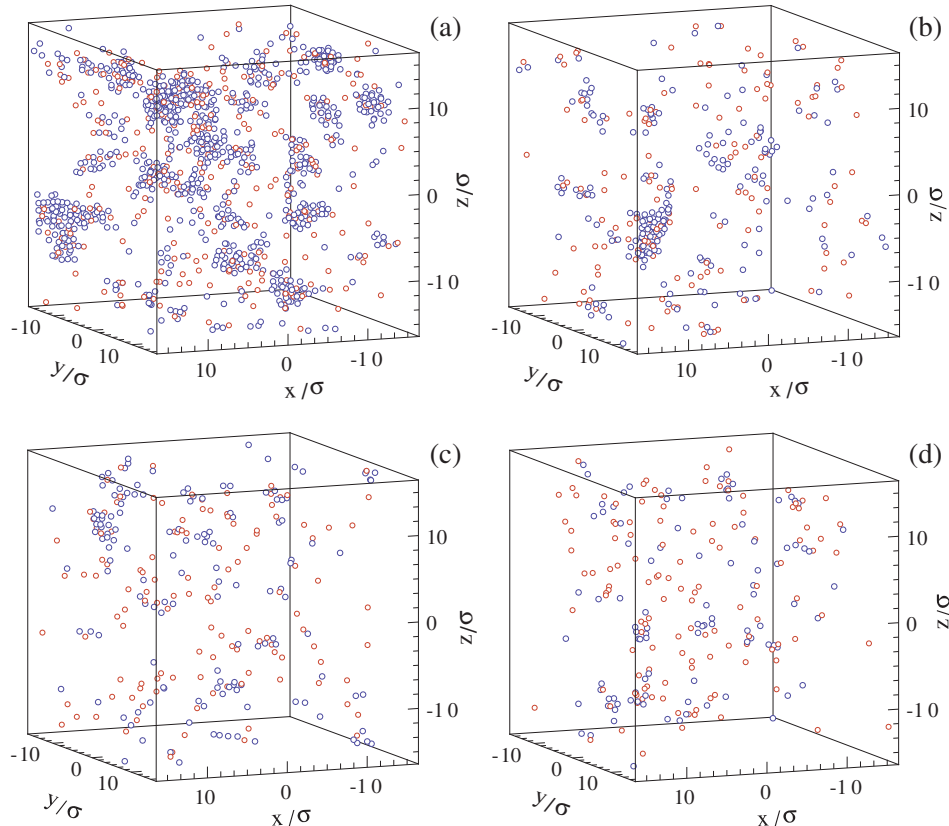

Fig. 6. Atomic configurations for the stress amplitude $\sigma_{zz}^{max} = 0.2\varepsilon\sigma^{-3}$ and nonaffine measure (a) $D^2(9T, T) > 0.04\sigma^2$, (b) $D^2(99T, T) > 0.04\sigma^2$, (c) $D^2(999T, T) > 0.04\sigma^2$, and (d) $D^2(4999T, T) > 0.04\sigma^2$.
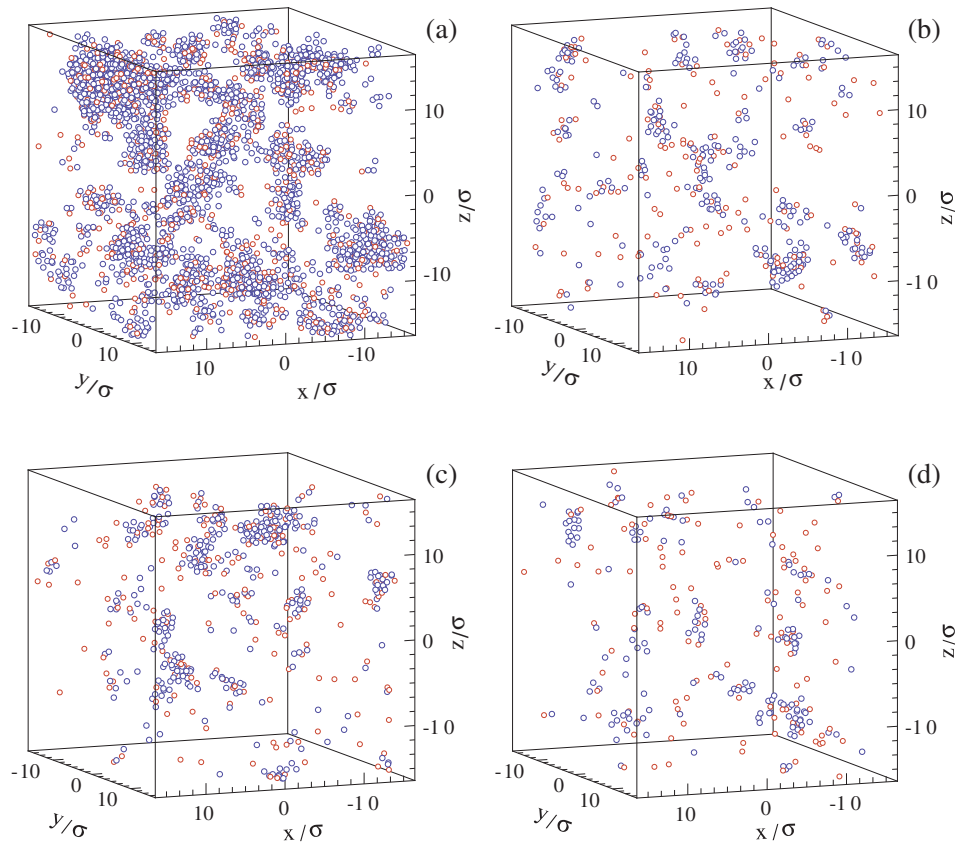
Fig. 7. Snapshots of atomic positions for the stress amplitude $\sigma_{zz}^{max} = 1.0\varepsilon\sigma^{-3}$ and nonaffine measure (a) $D^2(9T, T) > 0.04\sigma^2$, (b) $D^2(99T, T) > 0.04\sigma^2$, (c) $D^2(999T, T) > 0.04\sigma^2$, and (d) $D^2(4999T, T) > 0.04\sigma^2$.

represented by a non-additive binary mixture, which was rapidly cooled from a liquid state to a temperature well below the glass transition. The uniaxial tension-compression loading was applied periodically, while the pressure in lateral directions was kept constant. In such a setup, during thousands of cycles in the elastic regime, the systems continue relocating into the states with deeper potential energy minima and gradually become denser and stronger. It was found that under cycling loading with larger stress amplitudes, the samples become more dense, the minimum of the potential energy is lower, and the elastic modulus is reduced. Finally, the slow relaxation process is accompanied with the appearance of clusters of atoms with large nonaffine displacements, whose typical size becomes smaller as the number of cycles increases.

Acknowledgments

References

[1] W.H. Wang, The elastic properties, elastic models and elastic perspectives of metallic glasses, Prog. Mater. Sci. 57 (2012) 487.
[2] A.S. Argon, Plastic deformation in metallic glasses, Acta Metall. 27 (1979) 47.
[3] F. Spaepen, A microscopic mechanism for steady state inhomogeneous flow in metallic glasses, Acta Metall. 25 (1977) 407.
[4] M.L. Falk, J.S. Langer, Dynamics of viscoplastic deformation in amorphous solids, Phys. Rev. E 57 (1998) 7192.
[5] J. Ding, Y.-Q. Cheng, H. Sheng, M. Asta, R.O. Ritchie, E. Ma, Universal structural parameter to quantitatively predict metallic glass properties, Nat. Commun. 7 (2016) 13733.
[6] C.E. Packard, L.M. Witmer, C.A. Schuh, Hardening of a metallic glass during cyclic loading in the elastic range, Appl. Phys. Lett. 92 (2008) 171911.
[7] C. Deng, C.A. Schuh, Atomistic mechanisms of cyclic hardening in metallic glass, Appl. Phys. Lett. 100 (2012) 251909.
[8] D. Zhao, H. Zhao, B. Zhu, S. Wang, Investigation on hardening behavior of metallic glass under cyclic indentation loading via molecular dynamics simulation, Appl. Surf. Sci. 416 (2017) 14.
[9] H.R. Lashgari, C. Tang, D. Chu, S. Li, Molecular dynamics simulation of cyclic indentation in Fe-based amorphous alloy, Comput. Mater. Sci. 143 (2018) 473.
[10] S. Farhadi, A.Z. Zhu, R.P. Behringer, Stress relaxation for granular materials near jamming under cyclic compression, Phys. Rev. Lett. 115 (2015) 188001.
[11] M.M. Bandi, H.G.E. Hentschel, I. Procaccia, S. Roy, J. Zylberg, Training, memory and universal scaling in amorphous frictional granular matter, arXiv:1711.09382, 2018.
[12] Z.D. Sha, S.X. Qu, Z.S. Liu, T.J. Wang, H. Gao, Cyclic deformation in metallic glasses, Nano Lett. 15 (2015) 7010.
[13] Z. Sha, W.H. Wong, Q. Pei, P.S. Branicio, Z. Liu, T. Wang, T. Guo, H. Gao, Atomistic origin of size effects in fatigue behavior of metallic glasses, J. Mech. Phys. Solids 104 (2017) 84.
[14] Y.C. Lo, H.S. Chou, Y.T. Cheng, J.C. Huang, J.R. Morris, P.K. Liaw, Structural relaxation and self-repair behavior in nano-scaled Zr-Cu metallic glass under cyclic loading: Molecular dynamics simulations, Intermetallics 18 (2010) 954.
[15] Y. Shi, D. Louca, G. Wang, P.K. Liaw, Compression-compression fatigue study on model metallic glass nanowires by molecular dynamics simulations, J. Appl. Phys.

110 (2011) 023523.

[16] J. Luo, K. Dahmen, P.K. Liaw, Y. Shi, Low-cycle fatigue of metallic glass nanowires, Acta Mater. 87 (2015) 225.

[17] Y.F. Ye, S. Wang, J. Fan, C.T. Liu, Y. Yang, Atomistic mechanism of elastic softening in metallic glass under cyclic loading revealed by molecular dynamics simulations, Intermetallics 68 (2016) 5.

[18] D. Fiocco, G. Foffi, S. Sastry, Oscillatory athermal quasistatic deformation of a model glass, Phys. Rev. E 88 (2013) 020301(R).

[19] I. Regev, T. Lookman, C. Reichhardt, Onset of irreversibility and chaos in amorphous solids under periodic shear, Phys. Rev. E 88 (2013) 062401.

[20] I. Regev, J. Weber, C. Reichhardt, K.A. Dahmen, T. Lookman, Reversibility and criticality in amorphous solids, Nat. Commun. 6 (2015) 8805.

[21] T. Kawasaki, L. Berthier, Macroscopic yielding in jammed solids is accompanied by a non-equilibrium first-order transition in particle trajectories, Phys. Rev. E 94 (2016) 022615.

[22] P. Leishangthem, A.D.S. Parmar, S. Sastry, The yielding transition in amorphous solids under oscillatory shear deformation, Nat. Commun. 8 (2017) 14653.

[23] M.O. Lavrentovich, A.J. Liu, S.R. Nagel, Period proliferation in periodic states in cyclically sheared jammed solids, Phys. Rev. E 96 (2017) 020101(R).

[24] M. Fan, M. Wang, K. Zhang, Y. Liu, J. Schroers, M.D. Shattuck, C.S. O'Hern, The effects of cooling rate on particle rearrangement statistics: Rapidly cooled glasses are more ductile and less reversible, Phys. Rev. E 95 (2017) 022611.

[25] N.V. Priezjev, Heterogeneous relaxation dynamics in amorphous materials under cyclic loading, Phys. Rev. E 87 (2013) 052302.

[26] N.V. Priezjev, Dynamical heterogeneity in periodically deformed polymer glasses, Phys. Rev. E 89 (2014) 012601.

[27] N.V. Priezjev, Reversible plastic events during oscillatory deformation of amorphous solids, Phys. Rev. E 93 (2016) 013001.

[28] N.V. Priezjev, Nonaffine rearrangements of atoms in deformed and quiescent binary glasses, Phys. Rev. E 94 (2016) 023004.

[29] N.V. Priezjev, Collective nonaffine displacements in amorphous materials during large-amplitude oscillatory shear, Phys. Rev. E 95 (2017) 023002.

[30] S. Dagois-Bohy, E. Somfai, B.P. Tighe, M. van Hecke, Softening and yielding of soft glassy materials, Soft Matter 13 (2017) 9036.

[31] R. Ranganathan, Y. Shi, P. Keblinski, Commonalities in frequency-dependent viscoelastic damping in glasses in the MHz to THz regime, J. Appl. Phys. 122 (2017) 145103.

[32] N.V. Priezjev, Molecular dynamics simulations of the mechanical annealing process in metallic glasses: Effects of strain amplitude and temperature, J. Non-Cryst. Solids 479 (2018) 42.

[33] N.V. Priezjev, The yielding transition in periodically sheared binary glasses at finite temperature, Comput. Mater. Sci. 150 (2018) 162.

[34] W. Kob, H.C. Andersen, Testing mode-coupling theory for a supercooled binary Lennard-Jones mixture: The van Hove correlation function, Phys. Rev. E 51 (1995) 4626.

[35] T.A. Weber, F.H. Stillinger, Local order and structural transitions in amorphous metal-metalloid alloys, Phys. Rev. B 31 (1985) 1954.

[36] M.P. Allen, D.J. Tildesley, Computer Simulation of Liquids, Clarendon, Oxford, 1987.

[37] S.J. Plimpton, Fast parallel algorithms for short-range molecular dynamics, J. Comp. Phys. 117 (1995) 1.

[38] W. Kob, J.-L. Barrat, Aging Effects in a Lennard-Jones Glass, Phys. Rev. Lett. 78 (1997) 4581.

[39] W. Kob, J.-L. Barrat, Fluctuations, response and aging dynamics in a simple glass-forming liquid out of equilibrium, Eur. Phys. J.B 13 (2000) 319.